Nonlinear Resonant Acoustic Spectroscopy 10

Bart Van Damme and Koen Van Den Abeele

Contents

Abstract

Ultrasound nondestructive evaluation methods are popular since they are noninvasive, can be done by a trained technician, and can be used in situ. Pulse echo measurements with a single transducer and more advanced material examination using phased arrays allow for the detection of cracks and cavities in homogeneous materials. However, some types of damage remain invisible to traditional ultrasound nondestructive testing (NDT). Early stage fatigue damage, closed cracks, or delaminations in composites are typically difficult to discern. This chapter deals with the assessment of nonlinear wave distortion due to the presence of damage. In nonlinear elastic materials, resonance frequencies depend on the

B. Van Damme (✉)
Empa, Swiss Federal Laboratories for Materials Science and Technology, Dubendorf, Switzerland
e-mail: bart.vandamme@empa.ch

K. Van Den Abeele
Physics, Kulak Kortrijk Campus, Kortrijk, Belgium
e-mail: koen.vandenabeele@kuleuven.be

N. Ida, N. Meyendorf (eds.), *Handbook of Advanced Nondestructive Evaluation*,
https://doi.org/10.1007/978-3-319-26553-7_23

excitation amplitude. Nonlinear reverberation spectroscopy (NRS) exploits this small frequency shift in the ringing of a sample that was harmonically excited at resonance. Two successful applications are described. First, NRS was used to quantify thermal damage of carbon fiber reinforced polymers (CFRP) samples. The nonlinear parameters are much more sensitive to the microdamage than linear properties, such as a change of the Young's modulus or the damping coefficient. Moreover, the NRS results correlate well with optically gathered crack density values, and they can be modeled using a hysteretic elastic constitutive equation. The second example is the detection of early fatigue damage. A single closed crack in a steel sample can be exposed and even located when combining the NRS results with a finite element modal analysis.

Nonlinear Elasticity and Nondestructive Testing

Introduction

Traditional techniques for nondestructive testing (NDT), acoustical as well as others, are based on a contrast between the damaged zone and the intact material. This contrast can be a change in mechanical impedance, causing reflections and absorption of elastic waves (echography, sonar, acoustic scans) or a change in electromagnetic impedance (eddy current spectroscopy) (Mix 2005). When using ultrasound methods to assess materials, scale limitations arise. In general, the defect detection sensitivity increases for smaller wavelengths (Schmerr 2016). However, high frequency pulses are highly attenuated thereby limiting the application field. Sub-wavelength sized cracks can be detected by analyzing ultrasonic array signals, which requires costly equipment (Zhang 2016). Even then, there are certain cases where these techniques are not always successful. A single closed crack for instance establishes a particular problem for the strength of a material, but is nearly invisible for traditional acoustic techniques since an incoming wave is not reflected. A possible approach to overcome this problem is using nonlinear wave propagation properties of damaged materials (Guyer and Johnson 2009).

The phenomenon of nonlinear elastic behavior has been discovered as early as the eighteenth century, but its practical repercussions were only addressed halfway the twentieth century (Hamilton 1986). Whereas most homogeneous solid materials, like metals, show a linear stress-strain relationship, a lot of anomalies are known (Guyer and Johnson 2009; Nazarov and Radostin 2015). For large stresses in the elastic regime, the strain of most materials deviates from the linear Hooke's law. Other materials like sandstone show a strong nonlinear stress-strain relationship at much lower elastic stresses and even hysteresis when a stress cycle is applied. These effects have been investigated thoroughly over the past decades, and models were developed to describe the particular nonlinearity of different classes of materials.

Linear materials with local damage or with a distribution of microcracks show a higher nonlinear elastic behavior than an undamaged reference material (Van Den Abeele et al. 1997; Nagy 1998; Kim et al. 2011). In some cases where classical NDT

techniques fail, the measurement of a slight variation in the nonlinear material parameters can reveal early damage. The idea behind this concept is the fact that small cracks or delaminations are *activated* by the applied dynamic stress field, resulting in a response signal that is different from the expected response in the linear regime. The larger the activation energy, the larger the nonlinear response. The observation of this amplitude dependency will be used as an alternative for the classically used and widely spread commercial techniques available. Techniques based on nonlinear material behavior are commonly called nonlinear elastic wave spectroscopy (NEWS).

In this chapter, a short introduction to some widely used nonlinear material models is given first. The section is restricted to models necessary for the comprehension of the nonlinear NDT method. After an outline of the models, some examples of measurable footprints, produced by acoustic waves passing through nonlinear elastic zones, are given. The NEWS technique described in this chapter, nonlinear reverberation spectroscopy, are based on the detection of these nonlinear footprints.

Classical and Nonclassical Nonlinear Elasticity

Classical Nonlinearity

The relation between stress and strain determines the elastic modulus K, which is defined as

$$K = \frac{d\sigma}{d\epsilon}, \tag{1}$$

in which σ is the applied stress and ϵ is the strain. In linear materials, the elastic modulus is a constant K_0, resulting in Hooke's law

$$\sigma = K_0\epsilon. \tag{2}$$

The simplest case of nonlinear behavior can be described using a series expansion for the stress as a function of strain (Landau and Lifshitz 1959). This behavior can be described analytically as

$$\sigma = K_0\epsilon + K_0\beta^*\epsilon^2 + K_0\delta^*\epsilon^3 + \ldots \tag{3}$$

which can be rewritten using Eq. 1 as an elastic modulus

$$K = K_0\left(1 + \beta\epsilon + \delta\epsilon^2 + \ldots\right). \tag{4}$$

The perturbations $\beta\epsilon$ and $\delta\epsilon^2$ are typically much smaller than 1, and they describe the nonlinear hardening or softening of the material when a stress is applied. These perturbations are a function of the second and third (in the case of β) and even fourth (in the case of δ) order elastic constants of the material. When a sine wave is passing

through a medium and meets a zone governed by this constitutive relation, the original sine will be deformed and harmonics will be created. In case of first-order nonlinearity only, meaning that $\delta = 0$, even and odd harmonics show up in the resulting signal. When only second-order nonlinearity is present ($\beta = 0$), only odd harmonics will be created.

A material whose deformation is described by this relationship is called a *classical nonlinear* material. In linear elastic materials such as metals or Plexiglas without any damage, this nonlinear behavior is normally very small and difficult to measure. The sources of this nonlinearity however are well described and can be linked to deformations and dislocations at the atomic scale (Landau and Lifshitz 1959; Hamilton 1986). Classical nonlinearity is therefore also referred to as *atomic nonlinearity.* Since any material contains a certain amount of atomic defects, the nonlinear parameters will never be zero. It is important to know the natural nonlinearity level in order to quantify the influence of developing damage.

Nonclassical Nonlinearity: Hysteresis and the Preisach-Mayergoyz Approach

Micro-inhomogeneous materials like sandstone or concrete exhibit an even more complex demeanor when stress is applied. It has been known for a long time that rocks show a hysteretic behavior, comparable with the well-known hysteresis in ferromagnetic materials. When a cyclic stress is applied, the resulting strain exhibits a loop because of a different strain response when the material is compressed or stretched (Guyer and Johnson 1999). An example for sandstone is shown in Fig. 1.

As a result, the elastic modulus has discontinuities when the applied stress changes from positive to negative. In general, this can be described by

$$K = K(\epsilon, \dot{\epsilon}), \tag{5}$$

the time derivative $\dot{\epsilon}$ describing the dependency of the modulus on the direction in which the strain is varying, and its rate of change. When the strain diminishes, the value for K is different than when the strain increases. This dependency of the change of strain in time implies a memory effect of the hysteretic behavior. The memory shows up in the hysteretic curve in Fig. 1, where all inner loops arrive at the exact same place as where they started. This phenomenon is called endpoint memory, and it has been observed in a variety of materials.

More explicitly, the hysteretic stress-strain relation for a cyclic stress function can be described to first order by the equation

$$K(\epsilon) = K_0(1 - \alpha[\Delta\epsilon + \epsilon \ \text{sign}(\dot{\epsilon})]), \tag{6}$$

where $\Delta\epsilon$ is the amplitude during the last period and α is a constant describing the hysteretic behavior. The consequences of this elastic law for harmonic waves were described in a quasi-analytical way by Van Den Abeele et al. (1997). The most important result is that in this case of nonclassical nonlinear elasticity only odd harmonics are generated and that their amplitudes are proportional to the square of the fundamental strain amplitude.

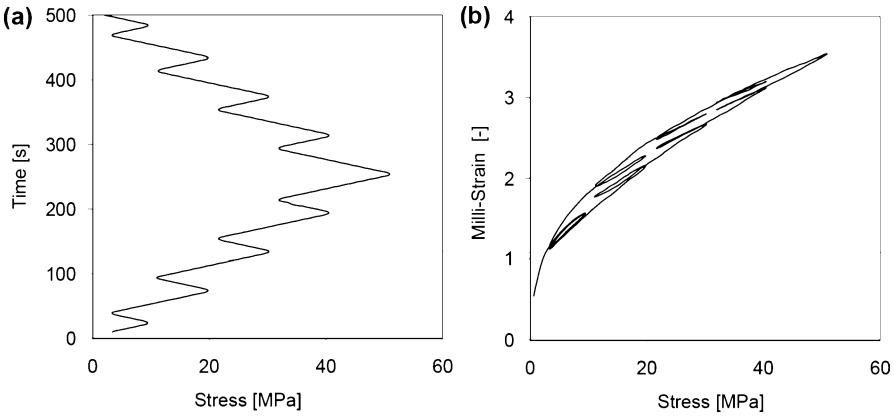

Fig. 1 Example of hysteretic behavior of Serena sandstone. The stress-strain relation (**b**) is shown for an applied stress protocol (**a**). Internal closed loops are visible

The physical explanation of this macroscopic behavior is commonly attributed to friction between the grains of a material (Walsh 1966; Mason 1969; Mavko 1979), although Sharma and Tutuncu (1994) found some discrepancies in this theorem and they added adhesion to this model. Most of these models however are purely descriptive, and very little analytical work is done (Pecorari 2004). All models however are based on the mesoscopic of materials. Mesoscopic refers to the scale between the nanolevel (atomic level, cf. classical nonlinearity) and the macroscopic properties, in this case the behavior of grains in stone or metals with a size varying from 0.1 to 10 μm. Since the bonds between the grains typically behave completely different than the material inside the grains, this results in nonclassical stress-strain relationships (Ten Cate and Shankland 1996; Darling et al. 2004).

A phenomenological approach to describe hysteresis is the use of the Preisach-Mayergoyz (PM) framework. This model was originally developed for the description of hysteresis in ferromagnetic materials but can also be used to deal with static and dynamic mechanical hysteresis (McCall and Guyer 1994; Guyer et al. 1995). The basis of this approach is to represent the material as an ensemble of features called hysterons. These entities can be either in an open or closed state. The stress value for which a hysteron opens (σ_o) or closes (σ_c) can be different for each individual hysteron. The strain caused by the opening of a single hysteron is assumed to be a constant value γ. The distribution of all hysterons can be represented in a space defined as a density of entities as function of the switching values σ_o and σ_c. This space is called the PM-space and the PM-space density $\rho_{PM}(\sigma_o, \sigma_c)$. This is represented schematically in Fig. 2.

The PM space, and the exact distribution of hysterons in particular, is usually applied as a purely mathematical tool to describe and model the hysteretic properties of a material. Some researchers however are investigating a universal theory about the physical grounds of the exact distribution of hysterons in PM space. Work is

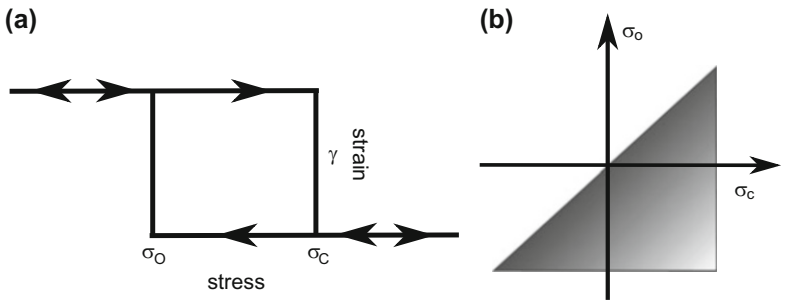

Fig. 2 Hysteron (**a**) and PM space distribution (**b**)

done by Aleshin and Van Den Abeele (2005, 2007, 2009) in the case of Hertzian friction between microscale material cells, but in most cases, a simple analytical distribution is used to approximate the reality. Some possibilities found in literature include a uniform distribution or an exponential distribution, scaled in such a way that the entire volume is equal to one. Experimental work on the dependency of the PM distribution on external factors such as humidity was done on concrete by Van Den Abeele et al. (2002).

The approach to calculate the strain from the stress is completely different than in the case of classical (nonlinear) elasticity and is only based on the amount of hysterons that are open and closed. The total strain of the medium is calculated as the amount of open hysterons, multiplied by the hysteron strain value γ. The amount of open and closed hysterons not only depends on the current stress and stress rate but on the entire history of the stress, on the initial states of the hysterons, and on the distribution of the hysterons in the PM space. The following example explains the procedure to calculate the strain for a certain stress cycle shown in Fig. 3a.

The PM space is represented in a plane defined by σ_c on the horizontal and σ_o on the vertical axis. The distribution of the hysterons in the PM space is situated in a triangular zone defined by the first bisector (for which $\sigma_c = \sigma_o$) and a horizontal and vertical line defining the maximum values of the opening and closing stresses. In theory, the vertical and horizontal limits of this zone can be infinite, but for practical calculations mostly finite borders are chosen. An example of the evolution of closed and open hysterons due to a predefined stress cycle is shown in (Fig. 3). In every situation, one single continuous line divides the set of open (on the upper right side) and the closed (on the lower left side) hysterons.

A purely hysteretic model does not take into account any classical elasticity. Most materials showing hysteretic behavior however can best be described using a combination of both hysteretic and classic elasticity. In for example sandstone, the sand grains can be seen as elastic building blocks of the material, whereas the bonds between the grains will behave in a hysteretic way. This model was, for instance, used in the simulation of resonant bars with localized damage (Van Den Abeele et al. 2004b).

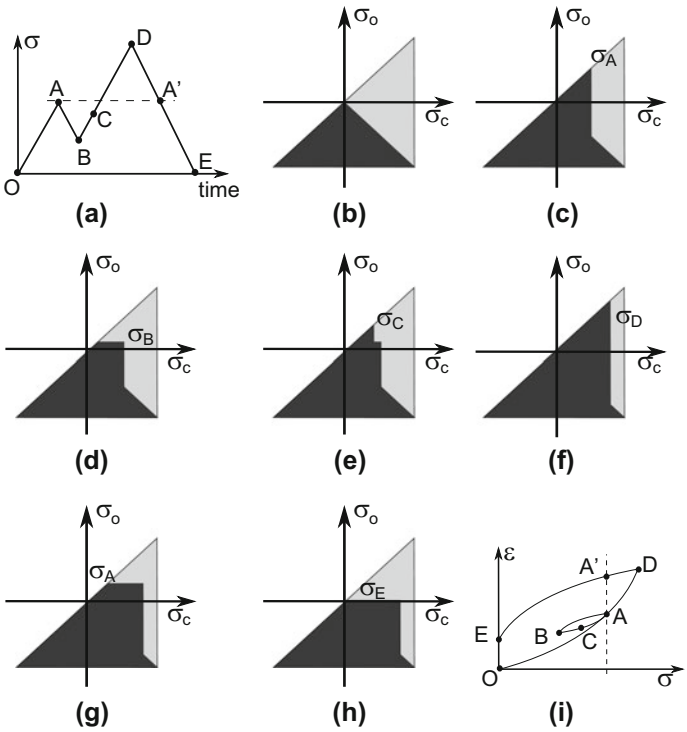

Fig. 3 Example of the evolution in PM space when applying the stress cycle shown in (**a**). The resulting strain can be seen in (**i**). The dark zone matches with closed hysterons, the lighter zone stands for open hysterons

Nonlinear Behavior of Damaged Materials

It is well known that the nonlinear elastic behavior of materials increases in the presence of damage, such as cracks (Nagy 1998; Van Den Abeele et al. 2000a, b). Early experiments using nonlinear methods for detecting small cracks in various materials such as steel, concrete, or carbon were performed by Antonets et al. (1986), Shkolnik (1993), Korotkov and Sutin (1994), Sutin et al. (1995). The exact physical basis of nonlinearity generation by cracks however is not completely understood, and a variety of models have been developed.

When applying a shear stress on a crack, both sides will slide. Mesoscopic friction models describe a stick-slip mechanism that is highly nonlinear. Theoretical investigations were done by Lawn and Brian (1998), Pecorari (2003), and more recently by Aleshin and Van Den Abeele (2007). Pecorari proved the presence of classical and hysteretic nonlinear effects, resulting in even and odd harmonics, respectively, whereas Aleshin related the contact of rough surfaces to a description of PM space distributions.

The nonlinearity of a sample is directly related to the damage state (Sutin et al. 2003; Gliozzi et al. 2006; Zumpano and Meo 2007); thus, the knowledge of the nonlinearity parameters can be used to detect and quantify the damage, and even to distinguish the type of damage from its specific nonlinear behavior (classical or hysteretic). Waves passing through the nonlinear elastic zones are distorted in a way that can be distinguished macroscopically. Most of these effects are based on amplitude dependent frequency changes and the generation of new frequencies in a sample when an external monochromatic sound wave is applied.

Harmonics generation The most direct effect of a nonlinear stress-strain relationship to assess damage is the generation of harmonics. Since the nonlinear contributions to the elastic modulus deform any sinusoidal wave traveling through a medium, harmonics will be generated. This approach has been successfully applied for cracks in aluminum samples (Buck et al. 1978; Morris et al. 1979) and carbon fiber-reinforced polymers (Kawashima et al. 2006; Solodov and Busse 2007).

Although the generation of harmonics is of large theoretical interest, experiments are often disturbed by nonlinear contributions from signal amplifiers that also deform sinusoidal signals. When using high amplitude excitation, it is therefore not easy to distinguish the harmonics produced by the damaged sample and the electronics used. Reference measurements on linear samples using the same electronic setup can be performed in order to filter out the erroneous effects.

Nonlinear wave modulation Another well-known nonlinear phenomenon is the mixing of two independent waves with frequencies f_0 and $f_1 (f_0 > f_1)$ when passing through a nonlinear medium. The waves interact, causing amplitude modulation effects. The resulting signal will not only consist of the original frequencies and their harmonics, but sideband frequencies $f_0 \pm f_1, f_0 \pm 2f_1, \ldots$ will also be created (Van Den Abeele et al. 2000b). The presence and amplitude of the sidebands depend on the type of nonlinearity.

The first experiments based on this particular nonlinear feature (nonlinear waveform modulation spectroscopy or NWMS) were performed in the 1990s by Sutin and Donskoy (1998). The technique is mostly used to detect cracks, for instance, by Courtney et al. (2008) and Zagrai et al. (2008), and for the evaluation of multilayered structures (Antonets et al. 1986). Kazakov et al. (2002) developed a way of localizing damage, comparable to the method described using harmonics detection.

Extensive work was done by Van Den Abeele et al. (2000b) in developing experiments to detect single cracks in Plexiglas and automotive parts. The authors were able to distinguish higher order modulation effects using a high frequency transducer and a low frequency shaker, and they compared the results with those of the harmonics detection. In the same paper, a method is described that uses a short impact (transient excitation) on the sample to produce a broadband low frequency signal consisting of the eigenfrequencies of the material. This technique is called impact modulation.

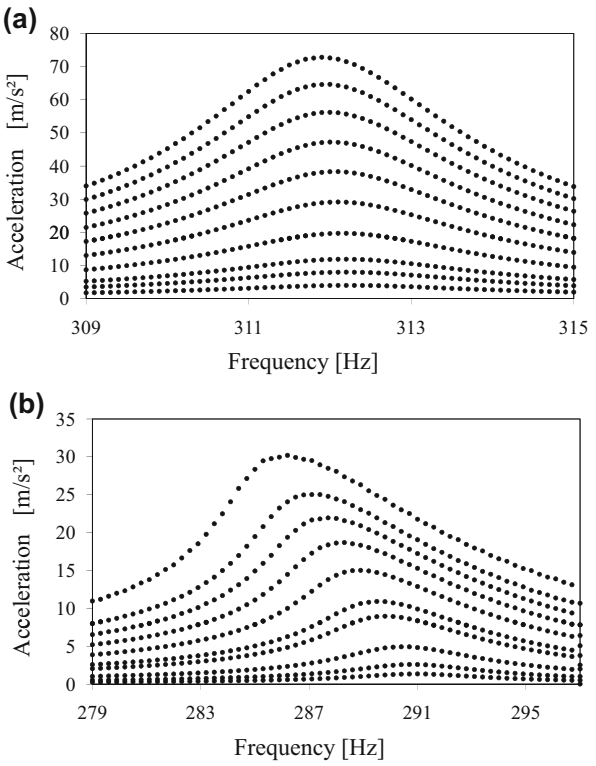

Fig. 4 Resonance curves of an intact (**a**) and damaged (**b**) slate beam sample measured for increasing driving amplitudes. (Reproduced from Van Den Abeele et al. 2000a, with the permission of the American Society for Nondestructive Testing, Inc.)

The main advantage of modulation effects over harmonics detection is the possibility of using independent wave sources for both signals. If there is no electronic connection between both sources, modulation frequencies can only be generated by the nonlinear material properties since no other nonlinear sources are present.

Amplitude-dependent eigenfrequency Since the eigenfrequencies of a material directly depend on the stiffness, an amplitude-dependent elastic modulus will result in an amplitude dependency of the eigenfrequencies. This phenomenon has, for instance, extensively been studied in inherently nonlinear materials, such as rocks (Johnson et al. 1996, 2004; Johnson and Sutin 2005) and for many other materials (Van Den Abeele et al. 2000a, 2006; Van Den Abeele and De Visscher 2000). The resonance frequency in sandstone shifts to lower values for increasing amplitudes. The nonlinear effect increases in damaged materials. An example is given in Fig. 4 for an undamaged and a damaged slate beam (Van Den Abeele et al. 2000a).

The authors developed a method of detecting damage based on the relative frequency shift, which they called Single Mode Nonlinear Resonance Acoustic/Ultrasound Spectroscopy (SiMoNRAS/SiMoNRUS). Resonance peaks are measured doing a step-by-step sweep over a fixed frequency range for increasing amplitudes.

This frequency domain method has shown to be effective for detecting damage in a variety of materials (Van Den Abeele et al. 2006), but the method is time consuming.

Slow dynamics It has been observed that the elastic properties of a material temporarily change after applying an elastic load. It is clear from the previous section that the resonance frequency of a sample decreases for larger amplitudes. In addition, after performing a SiMoNRAS experiment on sandstone at relatively high amplitude, a new sweep at low amplitude will result in a lower resonance frequency than was found in the original low amplitude sweep, which means the material has been softened by the previous high amplitude sweep. If the same frequency sweep at low strain amplitude is repeated, the resonance frequency shifts back toward its original value, indicating a relaxation in time of the material. This phenomenon is called slow dynamics.

Since slow dynamics is a proof of mesoscale nonlinearity, it can again be used for the detection of hysteretic features. Bentahar et al. (2006) and Johnson and Sutin (2005) compared fast (SiMoNRAS) and slow dynamic techniques for damage detection in concrete, both in a numerical way and experimentally. The authors found that damaged materials need much more time for the relaxation after applying a load, and the relative frequency change is much higher than in intact samples.

Nonlinear Reverberation Spectroscopy

Nonlinear resonance techniques investigate the conduct of objects when they are excited by increasing amplitudes. Generally, a single resonance mode of the object with its associated frequency is selected. In SiMoNRUS (Johnson et al. 1996; Van Den Abeele et al. 2000a), the object is subjected to a frequency sweep around this resonance frequency at constant excitation amplitude. The true resonance characteristics, frequency and damping (or quality factor), are then analyzed from fits of the resulting frequency response amplitude (resonance curve). Multiple resonances of complex objects can be exploited for a better estimation of the linear elastic properties.

The experiment can be repeated for increasing excitation amplitudes to analyze the nonlinearity of the object. Intact materials show no change in the resonance characteristics, whereas damaged materials generally show a decrease in the resonance frequency with amplitude (nonlinear softening) and an increase in the damping factor ($\pi f_0/Q$, with Q as the quality factor) due to nonlinear attenuation (Van Den Abeele and De Visscher 2000; Van den Abeele et al. 2002; Johnson and Sutin 2005).

Nonlinear reverberation spectroscopy (NRS) is the time domain analogy of SiMoNRUS. In NRS, a sample is excited using a constant excitation at a single frequency for a certain period of time. The frequency is chosen in the neighborhood of one of the resonance frequencies of the sample. After a number of cycles, sufficient to reach a steady-state response, the continuous wave excitation is stopped, say, at $t = t_0$. The reverberation response of the sample is measured from t_0 to t_1 and

stored for analysis. The recorded signal is a typical decaying time signal, with large amplitudes near t_0 and smaller amplitudes near t_1. This response is analyzed using a successive fitting of an exponentially decaying sine function,

$$A_k e^{-\xi_k t} \sin\left(2\pi f_k t + \phi k\right) \tag{7}$$

to small time windows (approximately 20 cycles). Here, A_k denotes the amplitude, ξ_k is the decay parameter, f_k is the frequency, and ϕ_k is the phase of the signal in the kth window. This allows the creation of a parametric plot of the true resonance frequency f_k and of the decay parameter ξ_k as a function of the amplitude A_k, thereby providing information on the occurrence of nonlinearity. If the material is linear, the frequency in different windows of the reverberation signal remains constant. If the material is nonlinear, the frequency in the reverberation signal gradually increases with decreasing amplitude and thus with time, in agreement with the nonlinear softening effect on the modulus due to the presence of nonlinearity (Guyer and Johnson 1999; Guyer et al. 1998).

SiMoNRUS and NRS can be performed in a fully noncontact mode by means of a loudspeaker as exciter and a laser Doppler vibrometer for the response measurement. The schematic setup and a typical NRS response and analysis of the data for one of the samples considered in section "Application to Thermally Loaded CFRP" (thermally shocked CFRP) can be found in Fig. 5a, b. The amplitude dependence of the resonance frequency and damping are clear markers of the nonlinear material behavior. When the amplitudes are recalculated in terms of strain (see section "NRS Results"), a NRS nonlinearity parameter can be deduced from the proportionality relation as the slope of the relative change.

Applications of NRS

Application to Thermally Loaded CFRP

CFRP and Heat Damage

Carbon fiber-reinforced polymers (CFRPs) are commonly used in the aircraft construction industry. It is expected that the next generation of airplanes will consist of more than 60% of composite structures (Taylor 2011). Even though composite materials hold important advantages over aluminum, CFRP is also prone to various degradation mechanisms. The exposure to heat, for instance, induces chemical and microstructural changes affecting the mechanical behavior of the composite laminate, even at moderate temperatures (Matzkanin 1999). Traditional nondestructive quality control techniques are often limited in their capabilities of detecting and characterizing subtle changes in the material properties associated with heat damage. A review of the mechanisms of heat damage in composites and a state of the art of nondestructive evaluation (NDE) techniques currently used to evaluate heat damage can be found in a comprehensive article by Matzkanin (1999).

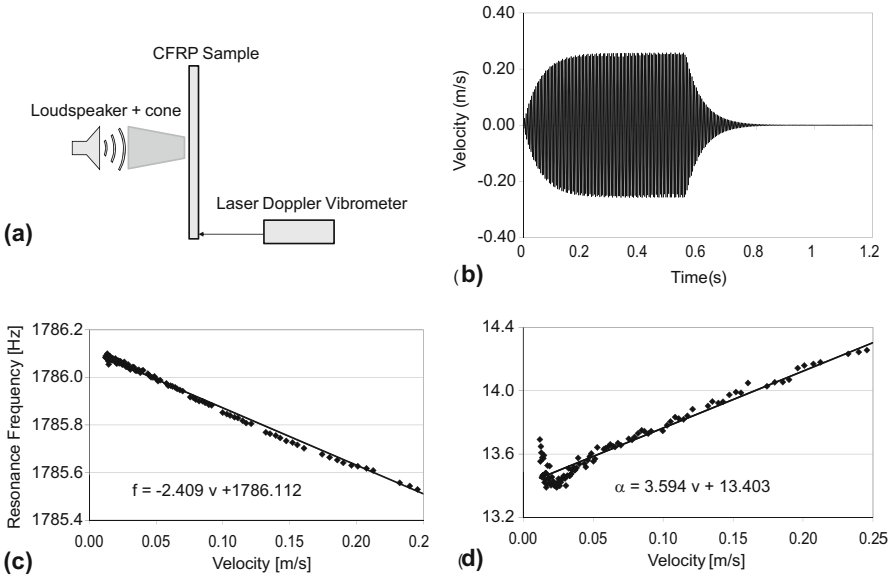

Fig. 5 NRS experimental setup (**a**) and typical results: (**b**) Full recorded signal; (**c**) Analysis of instantaneous resonance frequency versus particle velocity amplitude for a CFRP sample shocked at 300 °C for 30 min; (**d**) Analysis of instantaneous damping characteristic versus particle velocity amplitude for the same sample. (Reproduced from Van Den Abeele et al. 2009, https://doi.org/10.1121/1.3184583 with the permission of the Acoustical Society of America.)

Studies have shown that thermal degradation is typically matrix dominated since by the time fiber properties such as tensile strength and modulus are affected, all other mechanical integrity is lost. Mechanical metrics such as compressive, shear, and flexural strength and stiffness properties are believed to be the most sensitive properties for use in the early detection of thermal degradation, as opposed to nonmechanical parameters such as thermal and dielectric properties. Most of the work reported in the literature dealing with NDE for heat damage in composites deals with the following five methods: thermal (IR), ultrasonics, acoustic emission, dielectric properties, and radiography. These methods, while being readily available and well developed, are limited in their capabilities to detect and characterize the changes in composite material properties associated with heat damage. For instance, the detectability threshold of heat damage (1 h exposure at temperatures 200–300 °C in unidirectional AS4-8552 CFRP laminates using conventional ultrasonics (immersed transmission C-scan imaging at 5 MHz)) was found at 290 °C (Hyllengren 2001). This can be seen in the C-scan examples in Fig. 6. Nevertheless, the measured value of the interlaminar shear strength for the same type of samples changed from 121 MPa for nonexposed samples to 114 MPa when exposed at 200 °C, to 84 MPa for 285 °C, and to 43 MPa for samples exposed at 300 °C for the duration of 1 h.

Most traditional NDE techniques are capable of detecting physical anomalies such as cracks and delaminations. However, to be effective for thermal degradation, they must be capable of detecting initial heat damage, which occurs at a microscopic

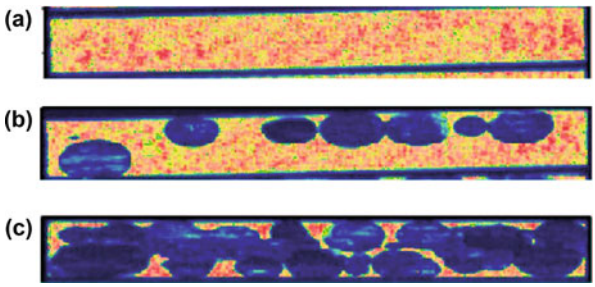

Fig. 6 Comparison of linear C-scan results for thermally loaded CFRP bars. The samples were exposed to 285 °C (**a**), 290 °C (**b**), and 300 °C (**c**) for 1 h. Delaminations (in dark blue) are only visible in the last two samples

scale. Review of the literature from more recent years indicates that a vast number of NDE methods are currently under development and show various degrees of promise for characterizing heat damage in composites.

NRS Results

We examined a set of heat damaged composite laminate samples using the above described NRS technique and quantified their NRS nonlinearity parameters as function of the heating temperature and exposure time. The set of 21 CFRP (AS4/8552 quasi-isotropic lay-up) samples consisted of one reference sample, which was left unexposed, and 20 samples exposed at five different temperatures (240, 250, 260, 270, and 300 °C) for four different durations (15, 30, 45, and 60 min). The samples were cooled under ambient conditions and tested at room temperature. The nominal size of the samples was 120 mm(L) × 20 mm (W) × 4 mm(T). It is expected that thermal damage is induced in a more or less uniform manner over the sample volume.

The resonance mode under consideration in this study (± 1800 Hz) is the fundamental flexural mode of a beam. It has a stress concentration in the middle of the sample and displacement nodes at a distance of 0.224L from both edges, with L as the length of the sample (120 mm) (Rayleigh 1896; Géradin and Rixen 1994). In the experimental setup, the sample is hung up by two nylon wires at the node lines and is excited at a pure tone by a loudspeaker (diameter of 32 mm the sound being concentrated by a converging cone of 180 mm length and 20 mm exit diameter) centered in the middle of the sample. The response is measured by a laser vibrometer (Polytec OFV303, decoder VD02) near one of the edges. All equipment is computer controlled and operated through LabVIEW and GPIB. The acquisition of the signal is realized by a PXI-5122 DAQ-card.

In the NRS experiment, the samples were excited by a 1000 period burst excitation at a given amplitude and with a frequency close to the fundamental flexural resonance frequency. The recorded signal was 0.6 s (120,000 points at a sampling rate of 200 kHz) of the reverberation of the sample after the excitation was stopped. Figure 5b shows a typical response from the start of the excitation to the steady state together with the reverberation. To achieve a high accuracy in the recording of the reverberation signal, a variable vertical range acquisition procedure was implemented based on an automated feedback of the instantaneous amplitude response. In this procedure, the dynamic range is decreased successively. At each

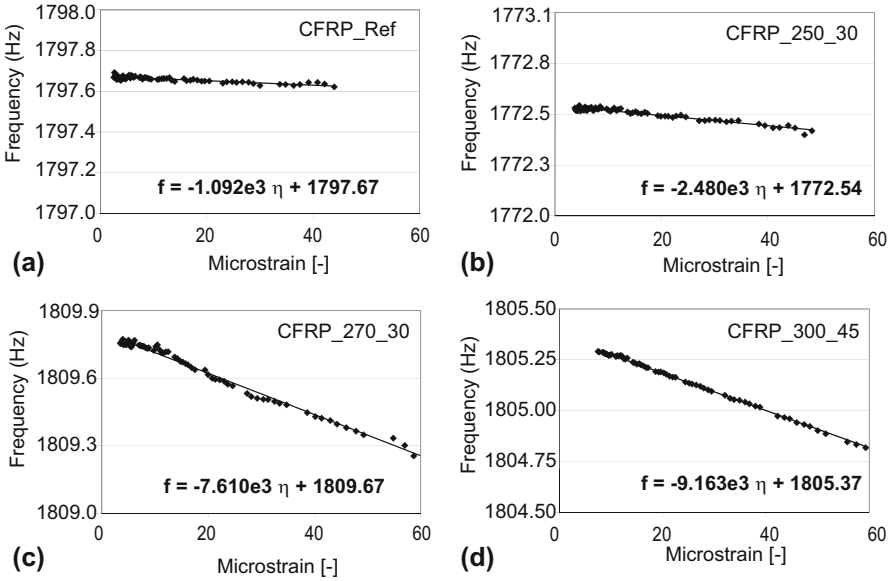

Fig. 7 NRS results showing the analyzed frequency versus microstrain amplitude for the reference sample (showing almost no nonlinearity) and for three samples submitted on beforehand to different heating temperatures and exposure times: 250 °C for 30 min, 270 °C for 30 min, and 300 °C for 45 min. (Reproduced from Van Den Abeele et al. 2009, https://doi.org/10.1121/1.3184583 with the permission of the Acoustical Society of America.)

range, signals are acquired and averaged ten times. The various signals recorded at decreasing dynamic range are finally matched to create a composed signal with adequate vertical resolution over the entire time axis. The amplitude, frequency, and damping information contained in the resulting signal are then analyzed by dividing the composed signal into several windows (with fixed time duration of 10 ms, which is typically of the order of 20 periodic oscillations) and by fitting the previously described exponentially decaying sine function (Eq. 7) to the data using a Levenberg-Marquardt algorithm to determine the parameters f_k, ξ_k, ϕ_k and A_k, with k referring to the kth time window. This yields the evolution of the frequency f_k and damping characteristic (ξ_k) as a function of the amplitude A_k in the decaying signal.

Figure 7 shows the results for the instantaneous resonance frequency versus amplitude for the reference sample (a), for two samples exposed for 30 min at 250 and 270 °C, respectively (b and c), and for a sample heated at 300 °C for 45 min (d). The analyzed data for the reference sample nearly follow a horizontal line, meaning that there is no or minimal dependence of the frequency on the amplitude. The reference sample is thus close to being a linear material. On the other hand, the results for longer exposure and higher temperature show an increased frequency dependence on amplitude, which indicates an increase in the material nonlinearity. Changing the window size for the analysis of the reverberating signal (within limits, of course) did not influence the results.

In order to quantify the degree of nonlinearity, the nonlinearity parameter Γ is defined as the proportionality coefficient between the relative resonance frequency shift and the strain amplitude $\Delta\epsilon$:

$$\frac{\Delta f}{f_0} = \Gamma \Delta\epsilon, \tag{8}$$

with f_0 as the linear resonance frequency and $\Delta f = f_0 - f_{res}$. The strain amplitude values, $\Delta\epsilon$, were calculated from the measured particle velocity amplitude values, v, using the strain-velocity conversion expression for beams (Géradin and Rixen 1994; Rayleigh 1896),

$$\Delta\epsilon \approx 0.219 \frac{T}{f\sqrt{12}} \left(\frac{4.73}{L}\right)^2 v \tag{9}$$

with thickness $T = 4$ mm and length $L = 120$ mm in the case of the used CFRP samples. It should be noted that because of the global character of the applied NEWS method, Γ only represents a global quantification of the nonlinearity, integrated over the whole sample. It contains no direct information on the localization of the defects. The values for the global NRS nonlinearity parameter Γ obtained in this study range from 0.6 to 6, and its variation as function of temperature and exposure time for all samples is summarized in Fig. 8a. We observed an overall increase with increasing exposure time and heat temperature up to a factor of 10 with respect to the reference value. The obtained values are comparable to values obtained for intact samples of heterogeneous materials such as slate (Van Den Abeele et al. 2000a), pultruded composites (Van Den Abeele et al. 2004a), concrete (Van Den Abeele and De Visscher 2000), and other materials (Johnson et al. 2004; Johnson and Sutin 2005).

A similar behavior can be observed when analyzing the nonlinearity in the damping characteristic,

$$\frac{\Delta\xi}{\xi_0} = \Upsilon \Delta\epsilon \tag{10}$$

with ξ_0 as the linear time constant (connected to the attenuation) leading to the damping nonlinear parameter Υ. However, the errors in the analysis results are larger (support of the samples is very critical for attenuation), and the linear fits are not as clean as the ones dealing with the resonance frequency shift, which results in a less pronounced evolution (Fig. 8c).

Comparison with the Linear Resonance and C-Scan Results and Discussion

The NRS analysis also provides the linear resonance signatures such as linear attenuation and linear resonance frequency. Ignoring subtle geometry changes, it is possible to calculate the global stiffness (Young's modulus E) for the different samples from the linear resonance frequency values. However, a systematic

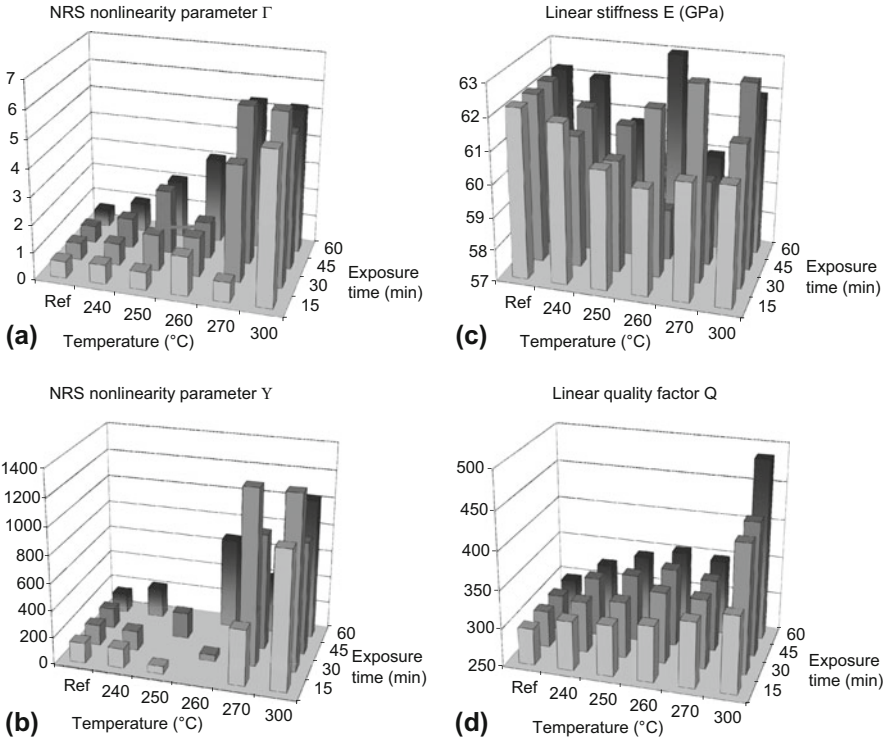

Fig. 8 Summary of the NRS results for all 21 samples as function of heating temperature and exposure time: (**a**) NRS nonlinearity parameter deduced from the frequency response, (**b**) NRS nonlinearity parameter deduced from the damping response (some Γ-values with low repeatability are omitted), (**c**) linear values of the stiffness E, and (**d**) linear Q-factor (inverse attenuation). The reference point was duplicated for different exposure times to help visualize the trend of the evolution of the parameters with temperature. (Reproduced from Van Den Abeele et al. 2009, https://doi.org/10.1121/1.3184583 with the permission of the Acoustical Society of America.)

change as function of the temperature and exposure time was not observed (Fig. 8b). For the attenuation, on the other hand, the linear value of the quality factor Q_0 (inverse attenuation $Q_0 = \pi f_0/\xi_0$) increases with temperature and exposure time (Fig. 8d), meaning that the attenuation (at that frequency) decreases with increasing damage.

It is obvious that the nonlinear parameters derived in the NRS method show a considerable gain in sensitivity and provide a consistent interpretation of the results in contrast with the linear characteristics. The NRS results also show to be more sensitive to heat damage than traditional C-scan results as shown in Fig. 6. For 1 h exposures, a clear variation of the nonlinearity Γ is noticed for temperatures as low as 250 °C, whereas the C-scan data only gives decisive damage information from 285 °C.

Quantification of the NRS Nonlinearity Parameter in Relation to the Microcrack Density

In order to compare the obtained values of the NRS nonlinearity parameter Γ with the microcrack density, five of the samples were sliced in the thickness direction and the crack density from each sample at the surface was calculated. To do so, the samples were imaged using light optical microscopy (LOM) coupled to a digital camera. Images are acquired with the magnification level set to 2. The process to quantify the crack density is described in detail in Van Den Abeele et al. (2009). In brief, the presence of cracks in layers with out-of-plane fiber orientation is determined analyzing gray-scale differences. In the selected areas, the crack-to-intact surface ratio, further referred to as crack density, is calculated.

The results of this treatment applied to all images lead to Fig. 9. Open diamonds represent the different values of the crack density obtained in several subsets of the images. The spread of the results is mainly due to the small size of the subset area, which is analyzed and illustrates the statistical variation as function of the position along the surface. As one can expect, some areas show almost no cracks, while others exhibit several of them. The filled circles are the average value for each sample. A clear relationship between the NRS nonlinearity parameter Γ and the crack density can be observed.

1. The NRS nonlinearity parameter increases with increasing crack density.
2. The dispersion of the data increases with the NRS nonlinearity parameter. This can be explained by the nonhomogeneous repartition of the cracks inside the samples.
3. Even though the crack density measurements for the reference sample and the sample treated at 250 °C for 60 min are not significantly different, a vast increase (more than a factor of 2) in the NRS nonlinearity parameter is observed. This could imply that the crack density procedure based on the image treatment is not sensitive enough to identify the very early features (e.g., increase in dislocation nuclei) that are responsible for the increased NRS nonlinearity parameter, even though they definitely exist. It again illustrates the extreme sensitivity of nonlinear techniques to early stages of damage.

Nonlinear Hysteretic Model

As mentioned in section "Nonlinear Elasticity and Nondestructive Testing," nonlinearity can be included by allowing the Young's modulus to depend on the stress and stress rates (and if necessary other history-dependent variables). In the following simulations, the PM approach, described in section "Nonclassical Nonlinearity: Hysteresis and the Preisach-Mayergoyz Approach," is used to take the nonlinearity into account. The free vibration of the first eigenmode of an Euler-Bernoulli beam was implemented using a finite difference Scheme. A (linear) constant damping coefficient was introduced using a relaxation time mechanism described in Blanch et al. (1995).

Upon performing the numerical simulations, the exact size and mass were measured for each sample, yielding input values for ρ and I. Five relaxation

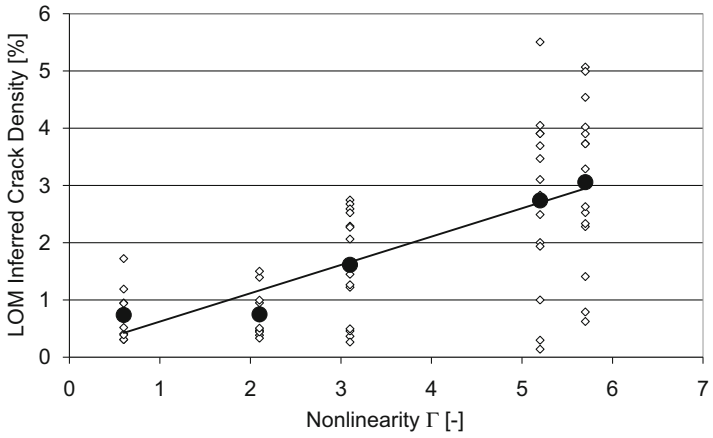

Fig. 9 Crack density in selected areas vs. NRS nonlinearity parameter Γ. Open diamonds are values of the crack density obtained for different parts of the images. Filled circles are the averages for the whole surface for each sample. The line is the linear trend line for the average values. The horizontal error bars for the experimentally obtained quantity of Γ are of a few percent for an individual sample. (Reproduced from Van Den Abeele et al. 2009, https://doi.org/10.1121/1.3184583 with the permission of the Acoustical Society of America.)

mechanisms are assumed to provide a constant Q_0 value over a broad frequency range (0.1–5000 Hz). Further, the linear value of the Young's modulus K_0 and the linear quality factor Q_0 are adjusted to obtain the correct low amplitude values for each sample. They are assumed to be uniform over the beam length. The nonlinearity is introduced by specifying the statistical distribution of the bistable PM elements. The simplest way, which is most commonly used for dynamic processes, is to assume a uniform distribution of the elements. In this case, only one parameter is needed. We call $\hat{\gamma}$ the PM background density parameter defined as

$$\hat{\gamma} = \rho_{PM}\gamma, \tag{11}$$

in which ρ_{PM} is the constant PM space density and γ is the strain contribution of one hysteron. The parameter $\hat{\gamma}$ is expressed in units of Pa^{-2}) (McCall and Guyer 1994; Guyer et al. 1995; Van Den Abeele et al. 2004b; Vanaverbeke and Van Den Abeele 2006) and its value is assumed to be uniform over the length of the sample (simulating a uniform distribution of damage). The physical meaning of the dimensionless quantity $\hat{\gamma} d\sigma_c d\sigma_o$ is that it represents the deformation contribution of the hysteretic elements in the PM space with opening pressures between σ_o and $\sigma_o + d\sigma_o$ and closing pressures between σ_c and $\sigma_c + d\sigma_c$ upon switching from one state to the other (open to closed or closed to open). The larger $\hat{\gamma}$, the larger the nonlinear strain contribution. This is the only free parameter to be used for fitting the nonlinear behavior.

The comparison of the results for an exposure to 300 °C for 30 min is shown in Fig. 10. The simulations track the experimentally observed resonance frequency

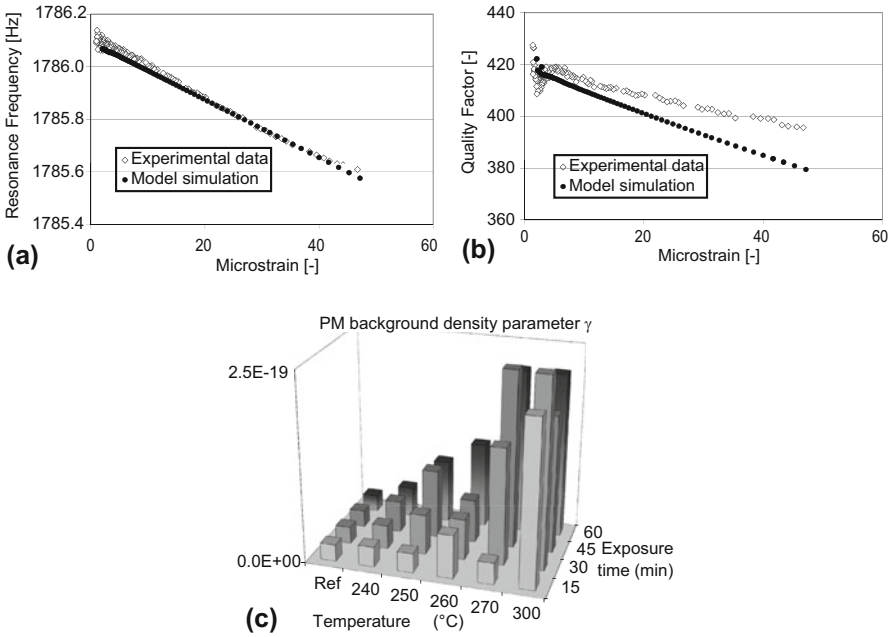

Fig. 10 Model results for CFRP_300_30 and comparison with experimental data: frequency (**a**) and quality factor (**b**). PM background density parameter γ used in the model simulations for all samples (**c**). The reference point was duplicated for different exposure times to help visualize the trend of the evolution of the parameters with temperature. (Reproduced from Van Den Abeele et al. 2009, https://doi.org/10.1121/1.3184583 with the permission of the Acoustical Society of America.)

reduction extremely well. For the nonlinearity in the damping, the experimental data are generally noisier. Nevertheless, it shows more or less the same tendency as was predicted in the simulations (with a 5% error at 50 microstrain). The discrepancy could be due to the nonideal support of the beams by the nylon wires located at the node lines in the experimental setup.

Three important issues about the nonlinearity parameter quantification should be noted.

1. The use of classical reversible nonlinear models, such as the polynomial expansion of stress versus strain (or vice versa) (Guyer et al. 1998), would lead to a quadratic behavior of the resonance frequency shift with amplitude and does not affect the attenuation characteristic. To find the linear decrease observed in the data for the resonance frequency and the quality factor Q, it is essential to start from a hysteretic model.
2. The PM background density parameter $\hat{\gamma}$ used in the numerical model is quite small. For the simulation of the nonlinear effects measured in the experiments, a value of $\hat{\gamma}$ between $2.2 \times 10^{-20}\text{Pa}^{-2}$ (reference sample) and $2.2 \times 10^{-19}\text{Pa}^{-2}$ (300 °C for 60 min) was used. As mentioned above, $d\sigma_c d\sigma_o$ represents the

deformation contribution of the hysteretic elements in the PM space with opening pressures between σ_o and $\sigma_o + d\sigma_o$ and closing pressures between σ_c and $\sigma_c + d\sigma_c$ upon switching from one state to the other. For a constant density in the statistical PM space, ranging from -5 to 5 MPa, this would amount to a total hysteretic contribution to the strain of only

$$\hat{\gamma} \int_{-5\ \mathrm{MPa}}^{5\ \mathrm{MPa}} \int_{-5\ \mathrm{MPa}}^{P_0} 1 d\sigma_c d\sigma_o = \hat{\gamma} \frac{1}{2} 10^{14} \tag{12}$$

$$\approx 10^{-6} - 10^{-5} \tag{13}$$

when changing the stress from -5 to 5 MPa.

3. Based on the PM space approach (McCall and Guyer 1994; Guyer et al. 1995; Van Den Abeele et al. 2004b; Vanaverbeke and Van Den Abeele 2006), the relative modulus change is – at first order of approximation – proportional to the constant background density parameter $\hat{\gamma}$ of the PM space, the linear modulus K_0, and the stress change itself. Since stress and strain are linked by the modulus, this results in

$$\frac{K_0 - K(\epsilon)}{K_0} \propto \hat{\gamma} K_0^2 \epsilon. \tag{14}$$

For those levels of nonlinear behavior observed in this study, giving rise to small frequency or modulus shifts, we indeed obtain in all cases a constant ratio between the macroscopically observed NRS nonlinearity parameter Γ and the theoretically found microscopic nonlinearity, which is expressed by the PM background density parameter γ:

$$\frac{\Gamma}{\hat{\gamma}} \left(\frac{12}{K_0} \right)^2 = 1. \tag{15}$$

Detection of Fatigue Damage in CFRP and Steel

Fatigue Damage in CFRP Bars

Damage induced by thermal shocking is generally quite small and uniformly distributed over the samples. Damage induced by fatigue loading can be more severe and is usually highly localized. NRS can also be applied to detect and quantify fatigue damage, which is highly localized. A zone of delaminations and cracks in fatigued CFRP beams, and a single surface breaking crack in a steel landing gear bracket are investigated.

The study on the fatigued CFRP samples shows a clear and sensitive signature of the nonlinearity (reduction of the frequency with amplitude, and increasing

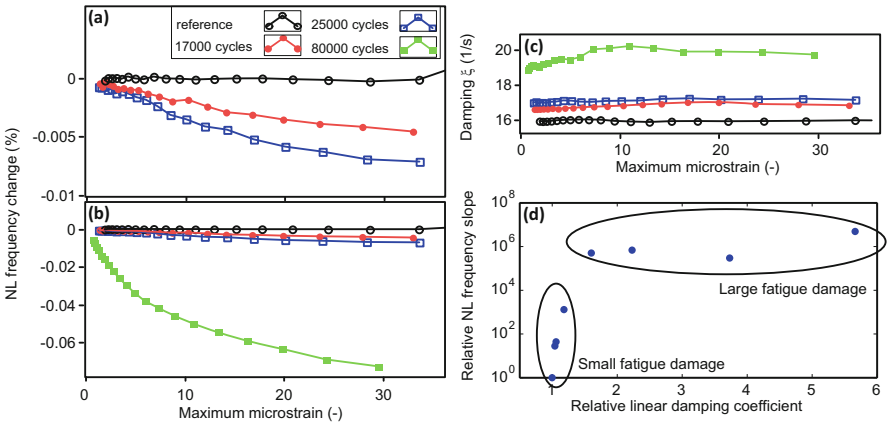

Fig. 11 Nonlinear frequency shift for mechanically damaged CFRP samples (reference sample and three samples with increasing number of fatigue cycles) (**a**, **b**). Damping coefficient for the same samples (**c**). Relative increase of nonlinearity (slope of the frequency change) as a function of the linear attenuation signatures, showing the sensitivity of nonlinear signatures over linear signatures for small damage (**d**). (Reproduced from Van Damme and Van Den Abeele 2014, https://doi.org/10.1007/s10921-014-0230-3 with the permission of the Springer Publishing Group.)

attenuation values) for different levels of damage (larger number of fatigue cycles), as can be seen in Fig. 11a, b. The frequency reduction is approximately linear in the case of a low number of fatigue cycles (<25000). However, to reach these nonlinear effects, the local level of microscopic nonlinearity $\hat{\gamma}$ at the localized damage zone must be far larger than in the case of thermal damage. Confining the zone of nonlinearity to a region of length $L/20$, centered in the beam, acceptable agreement with experiments requires simulation input values for$\hat{\gamma}$ of the order of 2×10^{-17} and higher, which is a factor 100 increase with respect to the thermally treated samples. When the number of fatigue cycles increases, secondary effects appear in the form of a reduced reduction rate and a stagnation of the frequency reduction (Fig. 11b). In the hysteretic PM space model this can be associated with a gradually decreasing population of the bistable elements in the statistical PM distribution, away from the PM space diagonal. This more complicated behavior cannot be described by a single parameter anymore. Similar effects are observed in the nonlinear attenuation.

The evolution of the linear damping parameter is consistent with the intuition that larger damage causes larger damping levels. The intercept at zero microstrain in Fig. 11c gradually provides a higher damping value for increasing fatigue cycles.

It is important to note, however, that the sensitivity of the nonlinearity signature is much larger than the sensitivity of a linear material property such as the attenuation, as can be appreciated from Fig. 11d. Additionally to the four previously described samples, four more fatigued samples were included in the analysis. Unfortunately, the fatigue history of these samples is unknown, but the damage is known to be much higher than the first series of four.

Fatigue Damage in a Steel Steering Actuator Bracket

The final example illustrates the NRS technique on a real industrial sample with a complex geometry: a steering actuator bracket, which is part of the nose landing gear of a commuter airplane. The bracket is made of POLDI L-ROL low alloy Czech steel (Czech standard CSN 14331). The sample is represented in Fig. 12.

Three samples with a different damage degree are used:

Bracket 1 was saved in intact state for comparison with brackets 2 and 3.

Bracket 2 had accumulated 11,185 pulsating stress cycles (stress ratio $R = 0$) using three point bending at a loading force level of 41,762 N. This level of the load caused a tensile stress about of 949 MPa in the critical point of the bracket according to strain gage measurement results. An estimation of crack growth

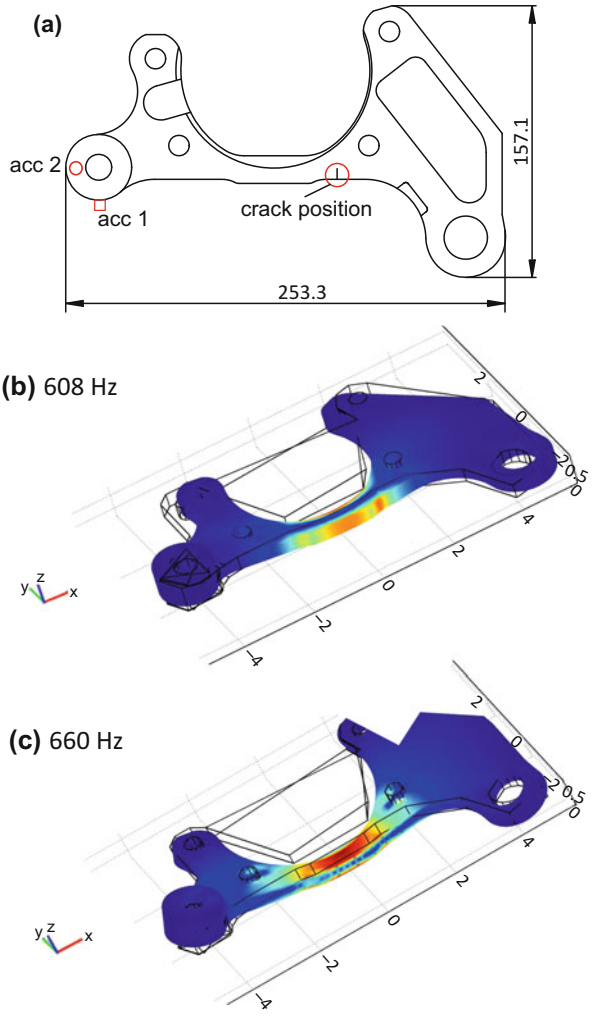

Fig. 12 Steering actuator bracket used as an industrial sample for the comparison of NEWS techniques. (Reproduced from Van Damme and Van Den Abeele 2014, https://doi.org/10.1007/s10921-014-0230-3 with the permission of the Springer Publishing Group.)

propagation was performed by calculations using the PREDIKCE code, VZLU in-house software (Aeronautical Research and Test Institute, Prague), and data obtained during fatigue loading of the bracket. The results of these calculations revealed inherent failure in the critical point of the bracket due to an initial crack. The estimated equivalent depth of the initial crack was about 0.7 mm.

Bracket 3 was fatigued using three point bending until a visible crack was present. It needed in total 123,808 loading cycles of 43,762 N. This level of the load caused a tensile stress about of 870 MPa in the critical point of the bracket according to strain gage measurement results. The existence of a 2.1 mm fatigue crack was confirmed by an eddy current system.

The shape and dimensions of the samples and the position of the fatigue crack is shown in Fig. 12. The massive steel body of the test specimen is about 12 × 15 mm in the zone of the crack location, which corresponds to the weakest point of the sample.

The experimental setup is essentially the same as for the CFRP samples except for the fact that the reception is made by means of an accelerometer (PCB Piezotronics 352B10). The results for the three samples are shown in Fig. 13. The experiment was performed twice, for two different eigenmodes of the bracket. Once again, there is a clear difference between the intact (red dots) and the damage bracket 1 (black squares). The measurement performed on the slightly damaged bracket 2 (green diamonds) is not decisive, as no significant difference with the undamaged bracket can be noticed. This is probably due to the fact that the single crack size is small compared to the applied wavelength, and the nonlinear wave distortion is too small to be measured. The scattering at low amplitude is due to the noise in the tail of the reverberation signal providing a bad resolution of the fits.

For this complex sample, with many vibration modes, the origin of the nonlinear wave distortion can be appreciated from the deformation shapes. The considered eigenmodes were modeled using finite element calculations. The von Mises stress

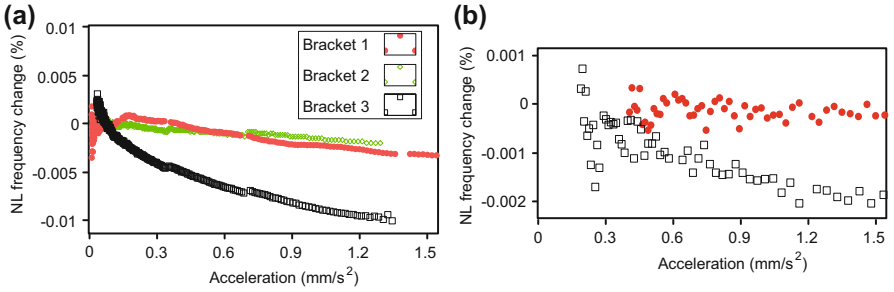

Fig. 13 NRS analysis (instantaneous normalized resonance frequency as function of the response amplitude) for an intact (bracket 1) and two damaged (bracket 2 and 3) steering actuator brackets for two frequencies: 609 Hz (**a**) and 681 Hz (**b**). (Reproduced from Van Damme and Van Den Abeele 2014, https://doi.org/10.1007/s10921-014-0230-3 with the permission of the Springer Publishing Group.)

for two modes is shown in Fig. 12. It is clearly visible that the first mode (607 Hz) is an in-plane bending mode, which allows the crack to open and close while vibrating. The second mode (660 Hz) is an out-of-plane torsional mode, which causes the crack's edges to slide over each other. It can be seen that the stress for both modes is large in the environment of the crack. Since the nonlinear frequency change of the first mode is much larger than the one of the second mode, one can assume that the first mechanism is more efficient than the second.

Discussion

NRS can be considered a time-domain version of the well-established nonlinear SiMoNRUS method, since both use the amplitude dependent eigenfrequency shift in order to quantify material nonlinearity. Figure 14 indicates the consistency between the two resonance methods applied to the first bending mode of a CFRP beam. The analyzed resonance frequency from the sweeps exhibits the same slope as the fitted resonance frequency deduced from the reverberation signal. There is a small offset related to a slight change in experimental conditions. The advantage of the NRS method is that it requires fewer acquisitions (one time signal at a single excitation level versus a discrete frequency sweep at various increasing levels of excitation) and, by such, that it is faster than SiMoNRUS.

For all thermally damaged samples and all moderately fatigued CFRP samples (less than 25,000 cycles), the results of the SiMoNRUS and NRS techniques are consistent, independent of the initial excitation amplitude. However, once the fatigue level is high, we systematically observed a difference between the sweep-based SiMoNRUS results obtained at increasing levels of excitation and the resonance frequency analysis from the reverberating signals for similar initial levels of the excitation. Figure 14b shows a clear example of this observation for a highly damaged sample. The circles, connected with lines, correspond to the NRS analysis at different external excitation levels. The red squares correspond to the peak resonance frequency in the SiMoNRUS analysis at exactly the same levels of

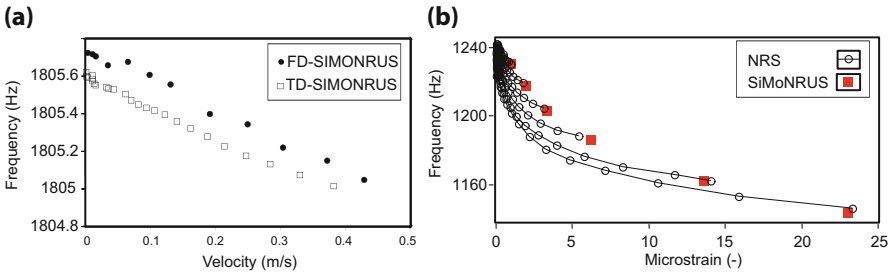

Fig. 14 Illustration of the agreement between the SiMoNRUS (circles) and NRS (squares) results. Heat treated CFRP (300 °C for 30 min) (**a**) and highly fatigued CFRP (**b**). (Reproduced from Van Damme and Van Den Abeele 2014, https://doi.org/10.1007/s10921-014-0230-3 with the permission of the Springer Publishing Group.)

external excitations. The highest amplitude data point of each NRS analysis matches quite well the results of the SiMoNRUS technique at the same excitation level.

The robustness of the method, a key feature for reproducible and trustworthy material evaluation, has been tested in several ways. Being a noncontact experiment, the only concern that could affect reproducibility is the string support of the sample. Paying particular attention to attach the supporting strings near the nodes of the resonance mode under consideration, several experiments were repeated after dismounting and remounting without invoking significant deviations in the results (errors of a few percent). In addition, even though experimental conditions may significantly affect the resonance frequency, the slope of the amplitude dependence, which yields the measure of the nonlinearity parameter in the NRS experiment, is independent of the exact resonance frequency value as it merely depends on the relative changes of it with respect to amplitude. These relative changes seem to be less dependent on the experimental conditions than the values of the resonance frequency. On top of this, we also verified that the obtained slope in the proportionality relations is independent of the chosen initial excitation frequency and applied voltage. The results of these investigations are illustrated in Fig. 15. In Fig. 15a, the response for three different frequencies close to the actual resonance frequency is illustrated for a fixed excitation amplitude. In Fig. 15b, the response at a fixed excitation frequency is illustrated for three different excitation amplitudes. This shows that the NRS nonlinearity parameter is independent of the initial excitation frequency (within limits in the order of the full width at half maximum of the resonance curve) and applied voltage (for regimes that do not involve slow dynamics). This insensitivity to changes in the experimental setup and conditions, in comparison to linear resonance measurements, is a practical advantage for the method.

In this chapter, the use of NRS was shown for two materials with very different properties, both regarding size, geometry, and material. Other researchers have further investigated the method, mainly to investigate the material nonlinearity due

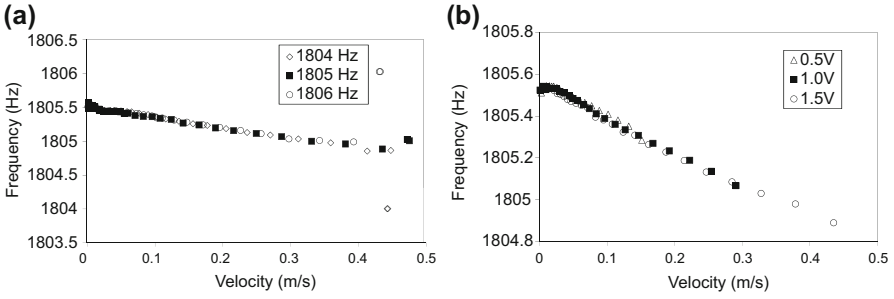

Fig. 15 Verification of the reliability of the NRS results for a single sample (CFRP_300_60) at various excitation frequencies (1804 Hz, 1805 Hz, 1806 Hz) for fixed amplitude (1.5 V) (**a**) and at various excitation amplitudes (0.5 V, 1 V, 1.5 V) for fixed excitation frequency (1805 Hz) (**b**). (Reproduced from Van Damme and Van Den Abeele 2014, https://doi.org/10.1007/s10921-014-0230-3 with the permission of the Springer Publishing Group.)

to scattered microdamage. Successful measurements were performed on bone (Haupert et al. 2014; Muller and Renaud 2011). The evaluation of concrete poses additional experimental difficulties, since the samples are too large to excite in a noncontact way using a loudspeaker. In this case, repeated hammer strokes with increasing force were successfully used to excite the first bending mode (Leśnicki et al. 2011; Jin et al. 2017).

Conclusion

In this chapter, a diagnostic technique for the detection of nonlinear material behavior was introduced and the efficiency of the NRS technique to detect damage was demonstrated. NRS is the time domain analogue of the SiMoNRUS technique, where the nonlinear amplitude dependent resonance frequency can be used to quantify material damage. Examples for global, heat induced, damage in CFRP beams were given, and a correlation was found between the nonlinear frequency changed and the optically measured crack density. This result confirms that the increase in nonlinearity is linked to an increased network of cracks and that the nonlinear signature is sensitive to microscopic alterations. Numerical simulations of bending resonances, using a hysteretic nonlinear constitutive relation within the sample support the results and relate the macroscopic NRS nonlinearity parameter to the microscopic PM background density of hysteretic elements (section "Nonlinear Hysteretic Model").

The technique was furthermore used for the detection of fatigue damage, both in CFRP beams and in a steel industrial sample (section "Detection of Fatigue Damage in CFRP and Steel"). The experiments prove that even the presence of a single fatigue crack shows up in the NRS results, if the crack is not too small. Due to the low frequencies used, and hence the large wavelengths present in the sample, a small single crack might be overlooked by this technique. In the complex shaped sample, the influence of the vibration mode on the NRS results was examined, showing that the NRS efficiency depends on the considered mode.

The NRS technique has the advantage to be fast, it has few or no restrictions on the sample geometry and in most cases it can be implemented in a fully noncontact manner (due to the low frequency nature of the method). On the other hand, it necessitates free (or at least steady, amplitude-independent) boundary conditions and is only applicable for low attenuation materials.

References

Aleshin V, Van Den Abeele K (2005) Micro-potential model for stress-strain hysteresis of microcracked materials. J Mech Phys Solids 53(4):795–824

Aleshin V, Van Den Abeele K (2007) Microcontact-based theory for acoustics in microdamaged materials. J Mech Phys Solids 55(2):366–390

Aleshin V, Van Den Abeele K (2009) Preisach analysis of the hertz-mindlin system. J Mech Phys Solids 57(4):657–672

Antonets V, Donskoy D, Sutin A (1986) Nonlinear vibro-diagnostics of flaws in multilayered structures. Mech Compos Mater 15(5):934–937
Bentahar M, El Aqra H, El Guerjouma R, Griffa M, Scalerandi M (2006) Hysteretic elasticity in damaged concrete: quantitative analysis of slow and fast dynamics. Phys Rev B 73(1):14,116
Blanch J, Robertsson J, Symes W (1995) Modeling of a constant-Q – methodology and algorithm for an efficient and optimally inexpensive viscoelastic technique. Geophysics 60(1):176–184
Buck O, Morris W, Richardson J (1978) Acoustic harmonic generation at unbonded interfaces and fatigue cracks. Appl Phys Lett 33(5):371–373
Courtney C, Drinkwater B, Neild S, Wilcox P (2008) Factors affecting the ultrasonic intermodulation crack detection technique using bispectral analysis. NDT & E Int 41(3):223–234
Darling T, TenCate J, Brown D, Clausen B, Vogel S (2004) Neutron diffraction study of the contribution of grain contacts to nonlinear stress-strain behavior. Geophys Res Lett 31:L16,604
Géradin M, Rixen D (1994) Mechanical vibrations: theory and application to structural dynamics, vol 25. Wiley, New York
Gliozzi A, Griffa M, Scalerandi M (2006) Efficiency of time-reversed acoustics for nonlinear damage detection in solids. J Acoust Soc Am 120:2506
Guyer R, Johnson P (1999) Nonlinear mesoscopic elasticity: evidence for a new class of materials. Phys Today 52:30–36
Guyer RA, Johnson PA (2009) Nonlinear mesoscopic elasticity: the complex behaviour of rocks, soil, concrete. Wiley, New York
Guyer R, McCall K, Boitnott G (1995) Hysteresis, discrete memory, and nonlinear wave propagation in rock: a new paradigm. Phys Rev Lett 74(17):3491–3494
Guyer R, McCall K, Van Den Abeele K (1998) Slow elastic dynamics in a resonant bar of rock. Geophys Res Lett 25(10):1585–1588
Hamilton M (1986) Fundamentals and applications of nonlinear acoustics, in nonlinear wave propagation in mechanics. The American Society of Mechanical Engineers, New York
Haupert S, Guerard S, Peyrin F, Mitton D, Laugier P (2014) Non destructive characterization of cortical bone micro-damage by nonlinear resonant ultrasound spectroscopy. PLoS One 9(1):e83,599
Hyllengren F (2001) Tech. Rep. No. TEK01-0022, C.S.M. Materialteknik, Linköping
Jin J, Moreno MG, Riviere J, Shokouhi P (2017) Impact-based nonlinear acoustic testing for characterizing distributed damage in concrete. J Nondestruct Eval 36(3):51
Johnson P, Sutin A (2005) Slow dynamics and anomalous nonlinear fast dynamics in diverse solids. J Acoust Soc Am 117:124
Johnson P, Zinszner B, Rasolofosaon P (1996) Resonance and elastic nonlinear phenomena in rock. J Geophys Res 101(B5):11,553–11,564
Johnson P, Zinszner B, Rasolofosaon P, Cohen-Tenoudji F, Van Den Abeele K (2004) Dynamic measurements of the nonlinear elastic parameter α in rock under varying conditions. J Geophys Res 109(B2):B02,202
Kawashima K, Murase M, Yamada R, Matsushima M, Uematsu M, Fujita F (2006) Nonlinear ultrasonic imaging of imperfectly bonded interfaces. Ultrasonics 44:e1329–e1333
Kazakov V, Sutin A, Johnson P (2002) Sensitive imaging of an elastic nonlinear wave-scattering source in a solid. Appl Phys Lett 81:646
Kim J, Jacobs L, Qu J (2011) Nonlinear ultrasonic techniques for nondestructive damage assessment in metallic materials. In: Fu-Kuo Chang (ed) 8th International workshop on structural health monitoring 2011: condition-based maintenance and intelligent structures. Department of Aeronautics and Astronautics, Stanford University, DEStech Publications, Incorporated
Korotkov A, Sutin A (1994) Modulation of ultrasound by vibrations in metal constructions with cracks. Acoust Lett 18(4):59–62
Landau LD, Lifshitz EM (1959) Theory of elasticity. Pergamon, Tarrytown
Lawn D, Brian R (1998) Nonlinear stress-strain curves for solids containing closed cracks with friction. J Mech Phys Solids 46(1):85–113
Lesnicki KJ, Kim JY, Kurtis KE, Jacobs LJ (2011) Characterization of asr damage in concrete using nonlinear impact resonance acoustic spectroscopy technique. NDT & E Int 44(8):721–727
Mason W (1969) Internal friction mechanism that produces an attenuation in the earth's crust proportional to the frequency. J Geophys Res 74(20):4963–4966

Matzkanin G (1999) Heat damage in graphite epoxy composites: degradation, measurement and detection. J Nondestruct Test Ultrason (Germany) 4(3). https://www.ndt.net/article/v04n03/ntiac/ntiac.htm
Mavko G (1979) Frictional attenuation: an inherent amplitude dependence. J Geophys Res 84 (B9):4769–4775
McCall K, Guyer R (1994) Equation of state and wave propagation in hysteretic nonlinear elastic materials. J Geophys Res 99(B12):23
Mix PE (2005) Introduction to nondestructive testing: a training guide, 2nd edn. Wiley, Hoboken
Morris W, Buck O, Inman R (1979) Acoustic harmonic generation due to fatigue damage in high-strength aluminum. J Appl Phys 50(11):6737–6741
Muller M, Renaud G (2011) Nonlinear acoustics for non-invasive assessment of bone micro-damage. In: Bone quantitative ultrasound. Springer, Dordrecht, pp 381–408
Nagy P (1998) Fatigue damage assessment by nonlinear ultrasonic materials characterization. Ultrasonics 36(1–5):375–381
Nazarov V, Radostin A (2015) Nonlinear acoustic waves in micro-inhomogeneous solids. Wiley, Hoboken
Pecorari C (2003) Nonlinear interaction of plane ultrasonic waves with an interface between rough surfaces in contact. J Acoust Soc Am 113:3065
Pecorari C (2004) Adhesion and nonlinear scattering by rough surfaces in contact: beyond the phenomenology of the preisach-mayergoyz framework. J Acoust Soc Am 116:1938–1947
Rayleigh B (1896) The theory of sound. Macmillan, London
Schmerr LW (2016) Probability of detection and reliability. Springer International Publishing, Cham, pp 685–695
Sharma M, Tutuncu A (1994) Grain contact adhesion hysteresis: a mechanism for attenuation of seismic waves. Geophys Res Lett 21(21):2323–2326
Shkolnik I (1993) Nondestructive testing of concretes: new aspects. Nondestruct Test Eval 10(6):351–358
Solodov I, Busse G (2007) Nonlinear air-coupled emission: the signature to reveal and image microdamage in solid materials. Appl Phys Lett 91(251):910
Sutin A, Donskoy D (1998) Vibro-acoustic modulation nondestructive evaluation technique. In: Proceedings of SPIE, vol 3397. International Society for Optics and Photonics, p 226
Sutin A, Delclos C, Lenclud M (1995) Investigations of the second harmonic generation due to cracks in large carbon electrodes. In: Proceeding of the 2nd international symposium on acoustical and vibratory surveillance methods and diagnostic techniques, Senlis, pp 725–735
Sutin A, Johnson P, TenCate J (2003) Development of nonlinear time reversed acoustics (nltra) for applications to crack detection in solids. In: Proceedings of the word congress of ultrasonics, pp 7–10
Taylor R (2011) Fiber composite aircraft-capability and safety. http://www.atsb.gov.au/media/27758/ar2007021.pdf
Ten Cate J, Shankland T (1996) Slow dynamics in the nonlinear elastic response of Berea sandstone. Geophys Res Lett 23(21):3019–3022
Van Damme B, Van Den Abeele K (2014) The application of nonlinear reverberation spectroscopy for the detection of localized fatigue damage. J Nondestruct Eval 33(2):263–268
Van Den Abeele K, De Visscher J (2000) Damage assessment in reinforced concrete using spectral and temporal nonlinear vibration techniques. Cem Concr Res 30(9):1453–1464
Van Den Abeele K, Johnson P, Guyer R, McCall K (1997) On the quasi-analytic treatment of hysteretic nonlinear response in elastic wave propagation. J Acoust Soc Am 101:1885–1898
Van Den Abeele K, Carmeliet J, TenCate J, Johnson P (2000a) Nonlinear elastic wave spectroscopy (NEWS) techniques to discern material damage, part II: single-mode nonlinear resonance acoustic spectroscopy. Res Nondestruct Eval 12(1):31–42
Van Den Abeele K, Johnson P, Sutin A (2000b) Nonlinear elastic wave spectroscopy (NEWS) techniques to discern material damage, part I: nonlinear wave modulation spectroscopy (NWMS). Res Nondestruct Eval 12(1):17–30

Van Den Abeele K, Carmeliet J, Johnson P, Zinszner B (2002) Influence of water saturation on the nonlinear elastic mesoscopic response in earth materials and the implications to the mechanism of nonlinearity. J Geophys Res 107(6):2121

Van Den Abeele K, Carmeliet J, Van De Velde K (2004a) Inferring the degradation of pultruded composites from dynamic nonlinear resonance measurements. Polym Compos 22(4):555–567

Van Den Abeele K, Schubert F, Aleshin V, Windels F, Carmeliet J (2004b) Resonant bar simulations in media with localized damage. Ultrasonics 42(1–9):1017–1024

Van Den Abeele K, Katkowski T, Wilkie-Chancellier N, Desadeleer W (2006) Laboratory experiments using nonlinear elastic wave spectroscopy (NEWS): a precursor to health monitoring applications in aeronautics, cultural heritage, and civil engineering. In: Universality of nonclassical nonlinearity, Springer, New York, pp 389–409

Van Den Abeele K, Le Bas P, Van Damme B, Katkowski T (2009) Quantification of material nonlinearity in relation to microdamage density using nonlinear reverberation spectroscopy: experimental and theoretical study. J Acoust Soc Am 126:963

Vanaverbeke S, Van Den Abeele K (2006) Multiscale approach for simulating nonlinear wave propagation in materials with localized microdamage. In: AIP conference proceedings, vol 838, p 91

Walsh J (1966) Seismic wave attenuation in rock due to friction. J Geophys Res 71(10):2591–2599

Zagrai A, Donskoy D, Chudnovsky A, Golovin E (2008) Micro-and macroscale damage detection using the nonlinear acoustic vibro-modulation technique. Res Nondestruct Eval 19(2):104–128

Zhang J (2016) Defect detection, classification, and characterization using ultrasound. In: Structural health monitoring (SHM) in aerospace structures. Elsevier, Amsterdam, pp 307–323

Zumpano G, Meo M (2007) A new nonlinear elastic time reversal acoustic method for the identification and localisation of stress corrosion cracking in welded plate-like structures-a simulation study. Int J Solids Struct 44(11–12):3666–3684